

The X-ray brightest clusters of galaxies from the Massive Cluster Survey

H. Ebeling¹, A.C. Edge², A. Mantz^{3,4}, E. Barrett¹, J. Patrick Henry¹, C.J. Ma¹, L. van Speybroeck⁵

¹ *Institute for Astronomy, University of Hawaii, 2680 Woodlawn Drive, Honolulu, HI 96822, USA*

² *Department of Physics, University of Durham, South Road, Durham, DH1 3LE, UK*

³ *Kavli Institute for Particle Astrophysics and Cosmology at Stanford University, 452 Lomita Mall, Stanford, CA 94305-4085, USA and SLAC National Accelerator Laboratory, 2575 Sand Hill Road, Menlo Park, CA 94025, USA*

⁴ *NASA Goddard Space Flight Center, Greenbelt, MD 20771, USA*

⁵ *Harvard-Smithsonian Center for Astrophysics, 60 Garden St, Cambridge, MA 02138, USA*

submitted December 2009

ABSTRACT

We present a statistically complete sample of very X-ray luminous galaxy clusters detected in the Massive Cluster Survey (MACS). This second MACS release comprises all 34 MACS clusters with nominal X-ray fluxes in excess of 2×10^{-12} erg s⁻¹ cm⁻² (0.1–2.4 keV) in the ROSAT Bright Source Catalogue; two thirds of them are new discoveries. Extending over the redshift range from 0.3 to 0.5, this subset complements the complete sample of the 12 most distant MACS clusters ($z > 0.5$) published in 2007 and further exemplifies the efficacy of X-ray selection for the compilation of samples of intrinsically massive galaxy clusters. Extensive follow-up observations with Chandra/ACIS led to three additional MACS cluster candidates being eliminated as (predominantly) X-ray point sources. For another four clusters — which, however, remain in our sample of 34 — the point-source contamination was found to be about 50%. The median X-ray luminosity of 1.3×10^{45} erg s⁻¹ (0.1–2.4 keV, Chandra, within r_{500}) of the clusters in this subsample demonstrates the power of the MACS survey strategy to find the most extreme and rarest clusters out to significant redshift. A comparison of the optical and X-ray data for all clusters in this release finds a wide range of morphologies with no obvious bias in favour of either relaxed or merging systems.

Key words: X-rays: galaxies: clusters — galaxies: clusters: general

1 INTRODUCTION

Clusters of galaxies have long been recognised to offer exceptional opportunities for cosmological and astrophysical studies of remarkable diversity. As the largest gravitationally bound entities in the universe, they are rare objects, originating from extreme overdensities in the primordial density field, and growing through continuous accretion as well as serial mergers into mass concentrations of $10^{14-15} M_{\odot}$ at the present epoch.

While in-depth studies of individual clusters are invaluable for our understanding of the physical processes governing the interaction between the three principal cluster constituents (dark matter, intracluster gas, and galaxies), it is only through observations of well defined, large samples of clusters that we can (a) obtain statistically meaningful information about the properties of clusters as a class of objects evolving on cosmological timescales, and (b) hope to find exceptional systems, such as, e.g., the Bullet Cluster (Markevitch et al. 2004; Bradač 2006; Clowe et al. 2006), that enable us to conduct quantitative measurements of fundamental astrophysical parameters. For many decades, such studies had to be

based on optically selected cluster samples which, while large, have the distinct disadvantage of being inherently affected and biased by projection effects (van Haarlem, Frenk & White 1997; Hicks et al. 2008).

A nearly unbiased way of selecting statistical cluster samples is through X-ray surveys, as the X-ray emission, which originates from the diffuse intra-cluster gas trapped in the clusters' gravitational potential well and heated to virial temperatures of typically 10^{7-8} K, represents direct proof of the existence of a three-dimensionally bound system. Also, the X-ray emission is much more peaked at the cluster centre than is the projected galaxy distribution, making projection effects in X-ray selected cluster samples highly improbable.

The advantage of X-ray cluster surveys over optical surveys is illustrated in Fig. 1 which compares the redshift histograms of the nine optically selected systems of the Palomar Distant Cluster Survey (PDCS; Oke, Postman & Lubin, 1998) with those of the twelve most distant X-ray selected MACS clusters (Ebeling et al. 2007). The severe contamination by fore- and background structures seen

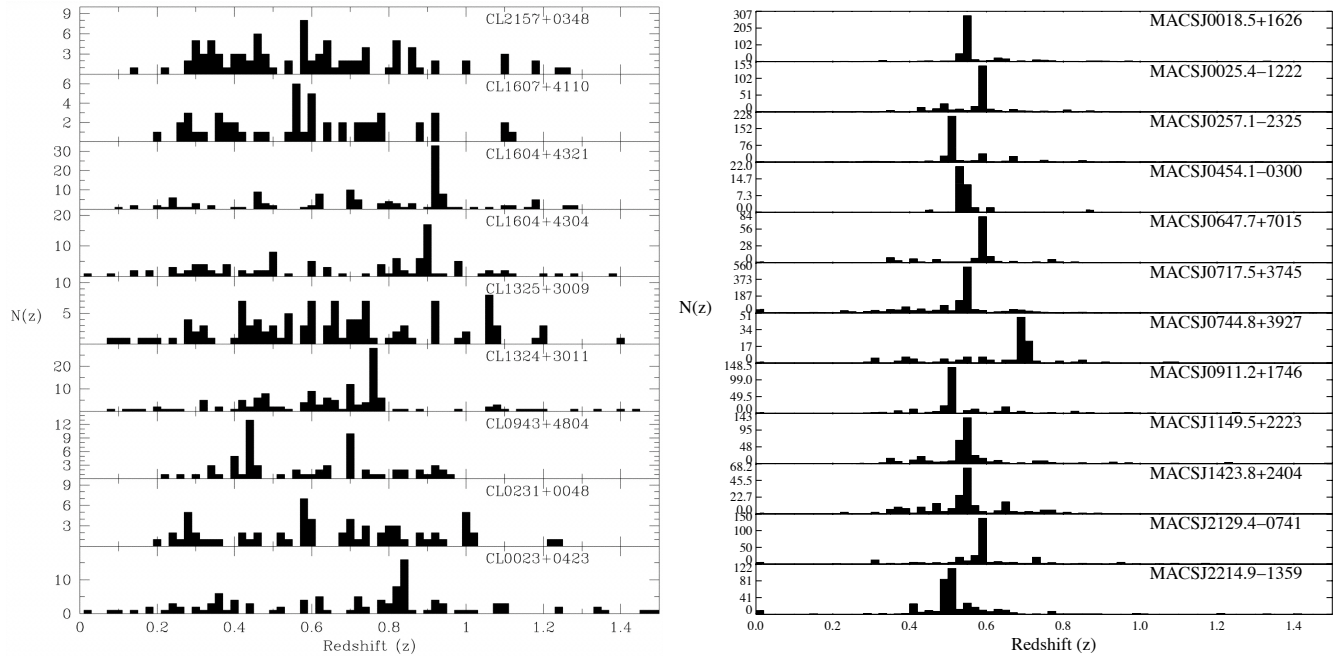


Figure 1. Histograms of galaxy redshifts in the fields of the nine optically selected systems of the PDCS (left; Oke et al. 1998) and the twelve most distant X-ray selected MACS clusters (right; Ebeling et al. 2007). For ease of comparison the MACS data are shown over the same redshift range and with the same binning as used in the published PDCS figure. Note that both surveys used similar criteria to select galaxies for spectroscopic follow-up observation.

in projection in the PDCS is endemic in optically selected cluster samples. Pure projection effects like, e.g., CL0231+0048 (Fig. 1, left) can be largely eliminated by including information on galaxy colors or redshifts (photometric or spectroscopic) in the original cluster detection phase. However, even the latest, state-of-the-art optical cluster samples remain biased, as they are prone to select intrinsically poor systems whose apparently compact cluster core, high optical richness, and high velocity dispersion are inflated by line-of-sight alignment and infall (Hicks et al. 2008; Horesh et al. 2009). By contrast, X-ray selected cluster samples are almost entirely free of projection effects since they, by virtue of the X-ray selection criteria, comprise exclusively intrinsically massive, gravitationally collapsed systems.

2 CLUSTERS IN THE ROSAT ALL-SKY SURVEY

Enormous progress has been made in the past decade in studies of clusters in the local universe ($z \leq 0.3$). The availability of large, representative, X-ray selected samples compiled from ROSAT All-Sky Survey (RASS, Trümper 1983) data (Ebeling et al. 1996, 1998, 2000; De Grandi et al. 1999; Ebeling, Mullis & Tully 2002; Crudace et al. 2002; Böhringer et al. 2004; Kocevski et al. 2007) has allowed greatly improved, unbiased measurements of the properties of clusters as an astronomical class of objects. Especially the ROSAT Brightest Cluster Sample (BCS, Ebeling et al. 1998, 2000) and the REFLEX sample (Böhringer et al. 2004) have been used extensively for studies of the local cluster population (e.g., Allen et al. 1992; Crawford et al. 1995, 1999; Ebeling et al. 1997; Hudson & Ebeling 1997; Edge et al. 1999, Smith et al. 2001; Schuecker et al. 2001; Allen et al. 2003; Kocevski et al. 2004, 2006; Smith et al. 2005; Stanek et al. 2006; Kocevski & Ebeling 2006; Atrio-Barandela et al. 2008; Kashlinsky et al. 2008).

At higher redshift, the Massive Cluster Survey (MACS),

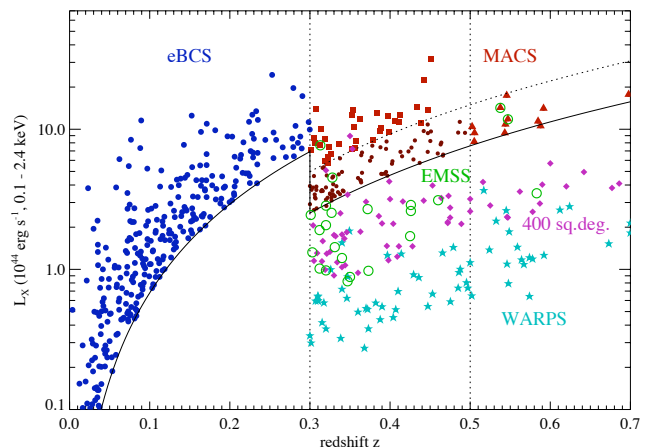


Figure 2. L_X - z distribution of clusters from various X-ray selected samples. By design MACS finds the high-redshift counterparts of the most X-ray luminous (and best studied) clusters in the local universe. Note also how MACS selects systems that are typically about 10 times more X-ray luminous, and thus much more massive, than those found in deeper serendipitous cluster surveys such as the EMSS, WARPS, or the 400 square-degree project. Two subsets of the MACS sample are highlighted: the sample presented here (red squares) and the 12 most distant MACS clusters at $z > 0.5$ (red triangles; Ebeling et al. 2007). A Λ CDM cosmology ($\Omega_M = 0.3$, $\Lambda = 0.7$, $h_0 = 0.7$) has been assumed.

launched in 1999, has compiled the first large X-ray selected sample of clusters that are both massive and distant. Based on sources listed in the RASS Bright Source Catalogue (BSC, Voges et al. 1999) MACS covers the entire extragalactic sky observable from Mauna Kea ($|b| > 20^\circ$, $-40^\circ \leq \delta \leq 80^\circ$), i.e. a solid angle of more than 22,000 deg², and focuses exclusively on clusters at

$z \geq 0.3$. An overview of the survey strategy is given by Ebeling, Edge & Henry (2001); the complete sample of the 12 most distant MACS clusters ($z > 0.5$) is presented in Ebeling et al. (2007). Comprising over 120 very X-ray luminous clusters, the MACS sample represents a 30-fold increase in the number of such systems known at $z > 0.3$. The $L_X - z$ distribution of the MACS sample is shown in Fig. 2 and compared to that of the BCS, EMSS, WARPS, and 400-sq.-deg. cluster samples (Ebeling et al. 1998, 2000; Gioia & Luppino 1994; Perlman et al. 2002; Burenin et al. 2007; Horner et al. 2008; Vikhlinin et al. 2009). Multi-wavelength, in-depth follow-up observations of MACS clusters in particular address a wealth of science issues across the full spectrum of extragalactic astronomy (LaRoque et al. 2003; Ruderman & Ebeling 2005; Smail et al. 2007; Stott et al. 2007, 2009; Ebeling, Barrett & Donovan 2004; Kartaltepe et al. 2008; Ma et al. 2008, 2009; Bradač et al. 2008; van Weeren et al. 2009; Ebeling et al. 2009; Bonafede et al. 2009; Smith et al. 2009; Limousin et al. 2009).

We here present the second complete subsample of MACS clusters comprising the 34 X-ray brightest systems. A Λ CDM cosmology with $\Omega_m = 0.3$, $\Omega_\Lambda = 0.7$ and $H_0 = 70 \text{ km s}^{-1} \text{ Mpc}^{-1}$ is assumed throughout.

3 THE 34 X-RAY BRIGHTEST MACS CLUSTERS

Two subsets of cluster candidates received special attention in the course of the compilation of the MACS sample: the most distant ($z > 0.5$) and the X-ray brightest. The former subset is discussed in Ebeling et al. (2007); we here present the second subsample, defined to comprise all MACS clusters with nominal (“detect”) fluxes¹ in the RASS BSC in excess of $2 \times 10^{-12} \text{ erg cm}^{-2} \text{ s}^{-1}$ (0.1–2.4 keV).

3.1 Cluster identification

Of the 5722 BSC sources meeting the general MACS selection criteria (see Ebeling et al. 2001), 2450 feature detect fluxes above the aforementioned limit. We identified all of these sources during a 6-year effort which involved repeated searches of the literature, visual inspection of optical images from public databases (Digitized Sky Survey and Sloan Digital Sky Survey), scrutiny of archival data from pointed X-ray observations conducted with ROSAT and Chandra, and – as the most time-consuming task – dedicated imaging and spectroscopic observations with the University of Hawai‘i 2.2m (UH2.2m) telescope and the Keck-II 10m-telescope.

In recognition of the fact that source identification efforts of this kind are bound to be subjective to some extent, we took great care not to give undue weight to the optical appearance of any BSC source. A balance has to be struck though. Although we did not use “optical richness” as a selection (or cluster confirmation) criterion, we required the presence of galaxies within the BSC error circle of approximately 2 arcmin diameter, eliminated sources coinciding with a single, bright, late-type galaxy, and, during spectroscopic follow-up, required at least two concordant galaxy redshifts of $z \geq 0.3$. Applying these optical cluster confirmation criteria in the most conservative fashion led to a first, tentative sample of 37 MACS

clusters with BSC detect fluxes exceeding the quoted limit. Multi-colour imaging in the V, R, and I passbands was performed with the UH2.2m telescope of all of these targets in order to allow an assessment of projection effects, and to enable the identification of potential stellar counterparts or contaminants of suspicious colour, such as (red) M stars or (blue) QSOs.

3.2 Chandra follow-up observations

MACS was designed to unveil the most X-ray luminous clusters of galaxies at intermediate redshift and to do so with the least possible bias. Although X-ray selected, the tentative sample of the 37 X-ray brightest MACS clusters is based on RASS detections of between 19 and 132 net photons (median: 54), far too few to allow a secure measurement of any X-ray characteristics beyond estimates of the source position and flux. Specifically, the existing RASS data do not permit us to assess whether the respective BSC sources are intrinsically extended and what fraction of the flux originates from point sources. In order to overcome both limitations, high-quality X-ray data were obtained with Chandra for all cluster candidates in this MACS subsample that had not been observed by Chandra at the time.

All Chandra data were analysed as described in detail in Mantz et al. (2010). Specifically, the normalisation of the Chandra fluxes was chosen such that the latter match those derived from pointed observations of the same targets with the ROSAT Position Sensitive Proportional Counter (PSPC). This approach is equivalent to using version 3.5.3 of the CXO calibration database².

Figure 3 demonstrates the ability of even very short Chandra ACIS-I observations (10 ks) to unambiguously identify the origin and nature of X-ray emission from cluster candidates at $z \geq 0.3$. We found two of the 37 clusters to contribute less than 10% of the X-ray flux detected, but not resolved, in the RASS; a third one (MACSJ1542.0–2915) turned out not to be a cluster at all. The relevant X-ray data for all three of these misidentifications (subsequently removed from the sample) are shown in the bottom panel of Fig. 3. The top panel of the same figure compares RASS and Chandra data for three confirmed clusters spanning the range of X-ray fluxes and redshifts of this MACS subsample. Fig. 3 illustrates two features of the RASS that are critically important for high-redshift cluster searches: (a) thanks to the low background of the ROSAT PSPC, even sources consisting of only a few dozen photons are detected at high significance in the RASS, and (b) dynamically relaxed clusters at $z > 0.3$ appear point-like. Both of these properties lie at the heart of the MACS strategy to use the faintest RASS sources — and no filter for apparent X-ray source extent — to find the most massive galaxy clusters out to increasingly high redshift.

3.3 The sample

The availability of Chandra data for all of the X-ray brightest MACS clusters enables accurate measurements of fundamental cluster properties such as X-ray flux, X-ray luminosity, and intra-cluster gas temperature. Even more importantly, and as a first for X-ray cluster surveys, our Chandra data allow us to remove X-ray point sources prior to the analysis for the entire sample. We list in Table 1 key properties of the 34 X-ray brightest MACS clusters as

¹ Prior to the identification of any RASS BSC sources we use an approximate conversion of the net count rate reported in the BSC to an unabsorbed X-ray flux by assuming that the observed X-ray emission originates from a hot, gaseous plasma with $Z = 0.3$ and $kT = 8 \text{ keV}$ at a redshift of $z = 0.2$.

² Updates to the effective areas used in Chandra CALDB version 3.5.5 break this agreement with the PSPC calibration, implying $\sim 14\%$ higher fluxes than earlier versions (Mantz et al. 2010).

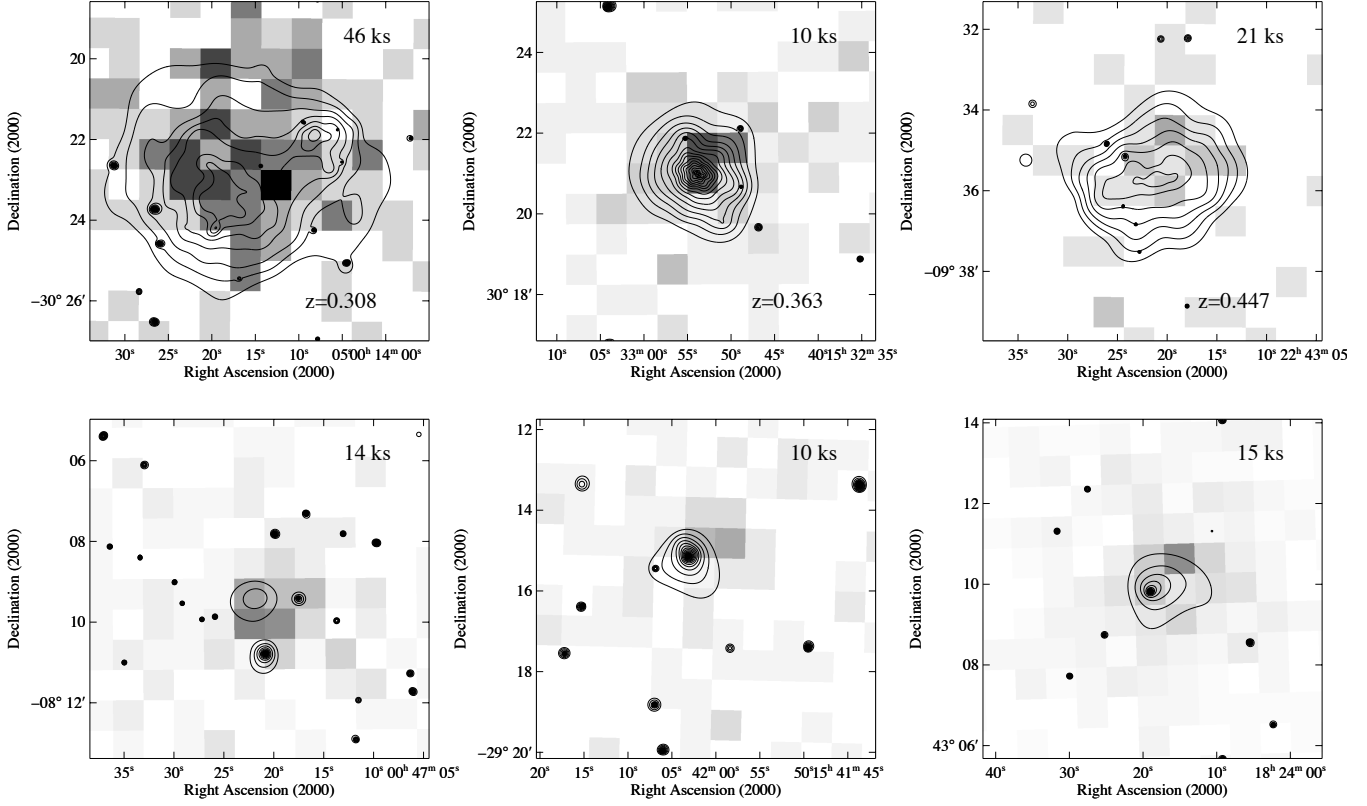


Figure 3. Contours of the X-ray surface brightness in the 0.5–7 keV band as observed with Chandra/ACIS-I overlaid on the RASS count-rate images (0.1–2.4 keV) of three confirmed MACS clusters (top row), and of the three erroneous identifications found to be dominated by X-ray point sources (bottom row). The intensity scaling is linear and the same for all six images; contours are spaced logarithmically at the same levels for all images. ACIS-I exposure times and cluster redshifts as labeled. The Chandra data were adaptively smoothed to 3σ significance using the ASMOOTH algorithm of Ebeling, White, and Rangarajan (2005). Note that, in the RASS, a distant virialized cluster like MACSJ1532.8+3021 ($z = 0.363$, top centre) appears just as point-like as the emission from a point source (bottom row).

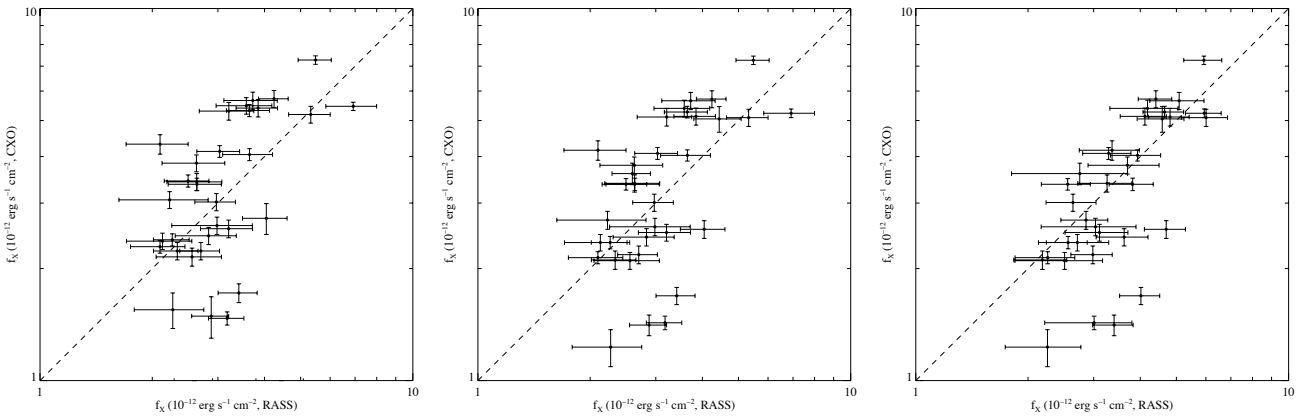


Figure 4. X-ray fluxes (0.1–2.4 keV) of the 34 X-ray brightest MACS clusters as derived from RASS and Chandra/ACIS observations. The left panel compares the Chandra measurements within r_{500} (including the contribution from X-ray point sources) to the RASS values as reported in the BSC (but corrected for aperture effects to match the Chandra measurement; see text for details). The middle panel shows the same comparison except that all X-ray point sources have now been removed from the Chandra measurements. Since point sources contribute, on average, only 3% of the Chandra flux values they are not primarily responsible for the large scatter. The right panel, finally, shows a visibly improved correlation when the point-source corrected Chandra fluxes are compared to RASS fluxes manually recomputed by us from the RASS raw data (within the same BSC detect cells and corrected for the same aperture effects). Apart from five outliers discussed in the main body of this paper, the recomputed RASS estimates are, within the errors, consistent with the Chandra measurements.

Table 1. Fundamental properties of the 34 X-ray brightest MACS clusters. We also list three misidentifications revealed by Chandra observations. All cluster redshifts were measured by us, unless noted otherwise. The listed coordinates correspond to the peak of the diffuse X-ray emission in our Chandra data, except for the X-ray point source MACSJ1542.0–2915 for which we list the optical position of the QSO. All X-ray fluxes and luminosities are measured in the 0.1–2.4 keV band. We list two fluxes determined from RASS data: the nominal “detect flux” listed in the RASS BSC (to be used with the MACS selection function provided in Table 2) and the flux within r_{500} as computed by us from the RASS raw data (see text for details). X-ray fluxes, luminosities, and gas temperatures determined from Chandra data are also computed within r_{500} and identical to the values listed in Mantz et al. (2010). X-ray morphology is assessed visually based on the appearance of the X-ray contours and the goodness of the optical/X-ray alignment. We use the same simple classification scheme as Ebeling et al. (2007), i.e. the assigned morphological classes (from apparently relaxed to extremely disturbed) are 1 (pronounced cool core, very good alignment of X-ray peak and single cD galaxy), 2 (good optical/X-ray alignment, concentric contours), 3 (non-concentric contours, obvious small-scale substructure), and 4 (poor optical/X-ray alignment, multiple peaks, no cD galaxy). From the differences between classifications made by different authors we estimate the uncertainty of the listed values to be less than 1.

MACS name	other name	α (J2000)	δ (J2000)	z	$n(z)$	$f_{\text{det,BSC}}^X$	$f_{r500,\text{RASS}}^X$	$f_{r500,\text{CXO}}^X$	$L_{r500,\text{CXO}}^X$	kT_{CXO} (keV)	morph. code
MACSJ0011.7–1523		00 11 42.9	–15 23 22	0.379	31	2.07 ± 0.34	2.23 ± 0.41	2.14 ± 0.08	8.9 ± 0.3	6.8 ± 0.6	1
MACSJ0014.3–3022	A2744	00 14 18.9	–30 23 22	0.308 ^a	n/a	5.42 ± 0.84	4.66 ± 0.51	5.23 ± 0.14	13.6 ± 0.4	8.5 ± 0.4	4
MACSJ0035.4–2015		00 35 26.5	–20 15 48	0.352	34	2.05 ± 0.34	2.54 ± 0.42	3.39 ± 0.18	11.9 ± 0.6	7.3 ± 0.7	3
MACSJ0152.5–2852		01 52 34.5	–28 53 36	0.413	30	2.72 ± 0.33	3.20 ± 0.39	1.69 ± 0.09	8.6 ± 0.5	4.7 ± 0.5	2
MACSJ0159.8–0849		01 59 49.4	–08 49 59	0.406	31	2.47 ± 0.34	2.53 ± 0.38	3.37 ± 0.12	16.0 ± 0.6	9.1 ± 0.7	1
MACSJ0242.5–2132		02 42 35.9	–21 32 26	0.314 ^b	1	3.74 ± 0.48	4.00 ± 0.57	5.13 ± 0.27	14.2 ± 0.8	5.0 ± 0.8	1
MACSJ0257.6–2209	A402	02 57 41.1	–22 09 18	0.322 ^c	n/a	2.22 ± 0.41	2.83 ± 0.45	2.43 ± 0.13	7.0 ± 0.4	7.0 ± 0.9	2
MACSJ0308.9+2645		03 08 55.8	+26 45 37	0.356	34	2.10 ± 0.40	3.36 ± 0.62	4.16 ± 0.25	14.7 ± 0.9	10.0 ± 1.1	4
MACSJ0358.8–2955		03 58 54.4	–29 55 32	0.425	13	2.65 ± 0.31	2.81 ± 0.97	3.60 ± 0.24	18.9 ± 1.2	8.8 ± 1.1	4
MACSJ0404.6+1109 ^d		04 04 33.3	+11 07 58	0.352	1	2.27 ± 0.48	2.26 ± 0.52	1.23 ± 0.14	4.3 ± 0.6	7.7 ± 2.8	4
MACSJ0417.5–1154		04 17 34.7	–11 54 33	0.443	41	4.13 ± 0.53	4.66 ± 0.66	5.09 ± 0.27	29.1 ± 1.5	9.5 ± 1.1	3
MACSJ0429.6–0253		04 29 36.0	–02 53 08	0.399	35	2.11 ± 0.42	2.68 ± 0.57	2.35 ± 0.12	10.9 ± 0.6	8.3 ± 1.6	1
MACSJ0520.7–1328		05 20 42.0	–13 28 50	0.336	2	2.51 ± 0.40	2.43 ± 0.47	2.50 ± 0.13	7.9 ± 0.4	6.5 ± 0.8	2
MACSJ0547.0–3904		05 47 01.5	–39 04 26	0.319	1	2.11 ± 0.26	2.34 ± 0.30	2.18 ± 0.12	6.4 ± 0.4	4.7 ± 0.5	2
MACSJ0947.2+7623	RBS 0797	09 47 13.0	+76 23 14	0.354	34	4.16 ± 0.38	4.32 ± 0.45	5.71 ± 0.30	20.0 ± 1.0	9.5 ± 2.1	1
MACSJ0949.8+1708	Z2661	09 49 51.7	+17 07 08	0.384	76	3.15 ± 0.43	3.66 ± 0.46	2.55 ± 0.14	10.6 ± 0.6	8.9 ± 1.8	2
MACSJ1115.8+0129		11 15 52.0	+01 29 55	0.355	50	2.98 ± 0.39	3.23 ± 0.48	4.08 ± 0.15	14.5 ± 0.5	9.2 ± 1.0	1
MACSJ1131.8–1955	A1300	11 31 54.4	–19 55 42	0.306	61	3.15 ± 0.53	4.72 ± 0.59	5.11 ± 0.28	13.1 ± 0.7	9.4 ± 1.7	4
MACSJ1206.2–0847		12 06 12.2	–08 48 01	0.439	46	2.04 ± 0.39	2.87 ± 0.62	3.79 ± 0.20	21.1 ± 1.1	10.7 ± 1.3	2
MACSJ1319.9+7003	A1722	13 20 08.4	+70 04 37	0.327	53	2.25 ± 0.26	2.66 ± 0.33	1.41 ± 0.09	4.2 ± 0.3	8.4 ± 2.4	2
MACSJ1347.5–1144	RX J1347.5–1145	13 47 30.6	–11 45 10	0.451	47	5.47 ± 0.56	5.91 ± 0.69	7.26 ± 0.19	42.2 ± 1.1	10.8 ± 0.8	1
MACSJ1427.6–2521		14 27 39.4	–25 21 02	0.318	43	3.09 ± 0.34	2.93 ± 0.77	1.43 ± 0.06	4.1 ± 0.2	4.9 ± 0.6	1
MACSJ1532.8+3021	RX J1532.9+3021	15 32 53.8	+30 20 58	0.363	61	3.58 ± 0.47	4.57 ± 0.57	5.27 ± 0.19	19.8 ± 0.7	6.8 ± 1.0	1
MACSJ1720.2+3536	Z8201	17 20 16.8	+35 36 26	0.387	62	2.24 ± 0.25	2.53 ± 0.32	2.35 ± 0.09	10.2 ± 0.4	7.9 ± 0.7	1
MACSJ1731.6+2252		17 31 39.1	+22 51 52	0.389	82	2.36 ± 0.32	2.21 ± 0.36	2.11 ± 0.12	9.3 ± 0.5	5.9 ± 0.6	4
MACSJ1931.8–2634		19 31 49.6	–26 34 34	0.352	35	3.65 ± 0.60	4.99 ± 0.83	5.65 ± 0.30	19.7 ± 1.0	7.5 ± 1.4	1
MACSJ2049.9–3217		20 49 56.2	–32 16 50	0.323	2	2.00 ± 0.40	1.96 ± 0.52	2.10 ± 0.11	6.1 ± 0.3	8.1 ± 1.2	3
MACSJ2140.2–2339	MS 2137.3–2353	21 40 15.2	–23 39 40	0.313 ^e	n/a	2.86 ± 0.44	3.08 ± 0.47	4.03 ± 0.14	11.1 ± 0.4	4.7 ± 0.4	1
MACSJ2211.7–0349		22 11 46.0	–03 49 47	0.397	27	2.78 ± 0.47	3.25 ± 0.67	5.39 ± 0.28	24.0 ± 1.2	14.0 ± 2.7	2
MACSJ2228.5+2036	RX J2228.6+2037	22 28 34.0	+20 37 18	0.411	35	2.26 ± 0.61	2.91 ± 0.42	2.70 ± 0.15	13.3 ± 0.7	7.4 ± 0.8	4
MACSJ2229.7–2755		22 29 45.2	–27 55 37	0.324	2	2.57 ± 0.42	3.72 ± 0.50	3.37 ± 0.13	10.0 ± 0.4	5.8 ± 0.7	1
MACSJ2243.3–0935		22 43 21.1	–09 35 43	0.447	36	2.31 ± 0.56	2.35 ± 0.67	2.59 ± 0.14	15.2 ± 0.8	8.2 ± 0.9	3
MACSJ2245.0+2637		22 45 04.6	+26 38 05	0.301	1	2.88 ± 0.36	2.56 ± 0.39	3.01 ± 0.16	7.6 ± 0.4	5.5 ± 0.6	1
MACSJ2311.5+0338	A2552	23 11 33.1	+03 38 07	0.305	22	3.48 ± 0.51	3.59 ± 0.52	5.05 ± 0.40	12.9 ± 1.0	7.5 ± 1.1	3
MACSJ0047.3–0810		00 47 21.8	–08 09 25	0.317	2	3.21 ± 0.36	AGN (6dF J0047208–081046; $z=0.1532$) at 00 47 20.83 –08 10 48.5 contributes > 90% of BSC flux				
MACSJ1542.0–2915		(15 42 03.10	–29 15 09.7)	–	n/a	2.72 ± 0.43	QSO				
MACSJ1824.3+4309		18 24 17.3	+43 09 56	0.483	12	3.19 ± 0.25	QSO at 18 24 19.01 +43 09 49.1 contributes 90% of BSC flux				

^a Struble & Rood (1999)

^b Wright, Ables & Allen (1983)

^c Romer (1994)

^d This system is a double cluster: the listed properties refer to the dominant south-western component

^e Stocke et al. (1991)

well as of the three cluster candidates found to be dominated by X-ray point sources.

Fig. 4 compares the unabsorbed X-ray fluxes determined from Chandra data to the corresponding estimates from the RASS. In order to minimize any model-dependent biases we do not extrapolate our measurements to larger radii to obtain “total” fluxes, but plot the Chandra fluxes measured directly within r_{500} , and the RASS fluxes measured directly within the BSC detect cell. Note, however, that we slightly adjust the BSC detect fluxes as listed in Table 1 to account for the small difference between r_{500} (median value for this sample: 4.4 arcmin) and the typical radius of the BSC extraction radius (5 arcmin), in the process accounting for the RASS point-spread function. Although this conversion requires the assumption of a β model (Cavaliere & Fusco-Femiano 1976), no significant systematic uncertainties are introduced as the resulting corrections are small (median correction: 4.5%). A straight comparison of the fluxes (including X-ray point sources) derived from Chandra and RASS-BSC data (Fig. 4, left) shows more scatter than expected given the size of the error bars. The middle panel of Fig. 4 illustrates that the large scatter is not caused by X-ray point sources. Although the Chandra data show the diffuse X-ray

emission from five clusters to be only about half as bright as suggested by the BSC fluxes³, X-ray point sources are found to contribute, on average, only 3% to the Chandra flux measurements within r_{500} . Unable to find other physical causes of the poor agreement, we investigated whether inaccurate RASS-BSC count rates might be to blame. Indeed, recomputing the source fluxes from the raw RASS data, within the original BSC detect-cell apertures and using a local background measured within an annulus extending from 3 to 4 Mpc (radius) at the cluster redshift, results in a visibly improved correlation with the Chandra fluxes (Fig. 4, right) and no systematic bias once the mentioned outliers are excluded ($f_{\text{RASS}}/f_{\text{Chandra}} = 1.0 \pm 0.2$).

The ability of the MACS project to find the most X-ray luminous galaxy clusters out to redshifts of $z \sim 0.5$ and beyond

³ For four of these (MACSJ0152.5–2852, MACSJ0949.8+1708, MACSJ1319.9+7003, and MACSJ1427.6–2521), the discrepancy can be attributed to bright X-ray point sources that fall within the RASS BSC detect cell; the fifth system (MACSJ0404.6+1109) features very extended diffuse emission, only part of which is captured by the Chandra measurement.

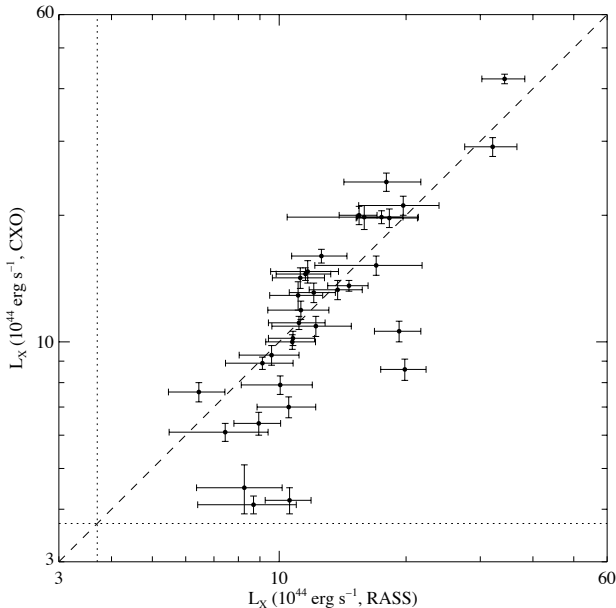


Figure 5. Comparison of X-ray luminosities (0.1–2.4 keV, within r_{500}) of the 34 X-ray brightest MACS clusters as derived from RASS and Chandra/ACIS observations. The RASS values are based on net count rates recomputed by us from the RASS raw data (see text for details); the Chandra measurements have been corrected for point-source contamination. The dotted lines mark the *total* X-ray luminosity of the Coma cluster in the same energy band.

has already been demonstrated by Ebeling et al. (2007) and is confirmed impressively here. We show, in Fig. 5, a comparison of the estimated RASS X-ray luminosities (using our recomputed count rates) with the values derived from Chandra observations. All systems feature X-ray luminosities (within r_{500}) in excess of 4×10^{44} erg s $^{-1}$ (0.1–2.4 keV) after correction for X-ray point sources, and are thus considerably more X-ray luminous than the Coma cluster ($L_X = 3.7 \times 10^{44}$ erg s $^{-1}$, extrapolated to the virial radius, Ebeling et al. 1998). The sample’s median X-ray luminosity is 1.3×10^{45} erg s $^{-1}$.

Fig. 6 shows overlays of the adaptively smoothed X-ray emission from all 34 clusters, as observed with Chandra, on colour images created from optical imaging in the V, R, and I passbands with the UH2.2m telescope in near-photometric conditions. This straightforward comparison of cluster morphologies in the optical and X-ray regime (see final column of Table 1 for a classification of X-ray morphologies) leads immediately to two conclusions: (a) MACS is not obviously biased in favour of either merging systems or cool-core clusters; (2) a large fraction of the clusters in our sample, including many systems without obvious cool cores, exhibit excellent alignment between the location of the brightest cluster galaxy and the peak of the X-ray emission. We discuss these findings in more detail in a separate paper (Mann & Ebeling, in preparation).

3.4 Selection function

In order to facilitate the use of the presented sample for cosmological applications, we list, in Table 2, the MACS selection function i.e. the solid angle covered by our survey as a function of RASS-BSC detect flux (as listed in Table 1). We limit the tabulated range

Table 2. MACS selection function. Listed are the RASS detect fluxes $f_{\text{det,BSC}}$ in units of 10^{-12} erg s $^{-1}$ cm $^{-2}$ in the 0.1–2.4 keV band and the solid angle in square degrees covered at fluxes exceeding $f_{\text{det,BSC}}$.

$f_{\text{det,BSC}}$	solid angle	$f_{\text{det,BSC}}$	solid angle	$f_{\text{det,BSC}}$	solid angle
2.00	21123	5.0	22297	14.0	22533
2.25	21432	5.5	22337	15.0	22541
2.50	21636	6.0	22369	17.5	22558
2.75	21775	6.5	22393	20.0	22569
3.00	21886	7.0	22414	22.5	22579
3.25	21971	7.5	22430	25.0	22584
3.50	22047	8.0	22446	27.5	22589
3.75	22116	9.0	22469	30.0	22594
4.00	22167	10.0	22488	35.0	22601
4.25	22213	11.0	22502	40.0	22607
4.50	22246	12.0	22514	45.0	22614
4.75	22277	13.0	22525	50.0	22617

to $f_{\text{det,BSC}} \geq 2 \times 10^{-12}$ erg s $^{-1}$ cm $^{-2}$ as the nominal RASS fluxes for yet fainter sources may be affected by the systematic effects illustrated in Fig. 4.

4 SUMMARY

We present the second statistically complete MACS subsample, comprising the 34 clusters with X-ray detect fluxes in excess of 2×10^{-12} erg s $^{-1}$ cm $^{-2}$ (0.1–2.4 keV) in the RASS Bright Source Catalogue. All clusters feature redshifts of $z \geq 0.3$, and 22 of the 34 are new discoveries. Chandra observations of the entire sample confirmed the cluster origin of the emission and allowed the elimination of three additional candidates whose X-ray emission was found to be dominated by point sources.

A comparison of the appearance of MACS clusters in the RASS and in Chandra observations confirms that all but the most disturbed clusters at $z > 0.3$ appear point-like at the angular resolution of the RASS. We find the original RASS count rates as listed in the BSC to be less accurate than manual measurements within the BSC aperture and using a local annulus for background subtraction. RASS fluxes based on recomputed count rates are in good agreement with the respective Chandra values, except for four clusters for which the RASS count rate is significantly contaminated by point sources within the BSC detect cell, and one system whose very extended emission is not fully captured by the Chandra measurement. For the remainder of the sample, X-ray point sources contribute, on average, only about 3% to the flux within r_{500} . All clusters of this second MACS subsample feature X-ray luminosities (within r_{500}) in excess of 4×10^{44} erg s $^{-1}$ (0.1–2.4 keV) after correction for X-ray point sources, and are thus considerably more X-ray luminous than the Coma cluster. The sample’s median X-ray luminosity of 1.3×10^{45} erg s $^{-1}$ confirms the efficiency of our survey technique to identify massive clusters well beyond the redshift limits of previous RASS-based cluster surveys. A first assessment of the optical and X-ray morphology of the clusters in this sample finds both fully virialized and heavily disturbed systems to be well represented, arguing against a strong bias in favour of either cool-core clusters or extreme mergers. A more quantitative analysis and discussion of the morphology and relaxation state of MACS clusters will be presented in a forthcoming paper.

When combined with the most X-ray luminous clusters in the local Universe ($z < 0.3$) from the eBCS and REFLEX surveys

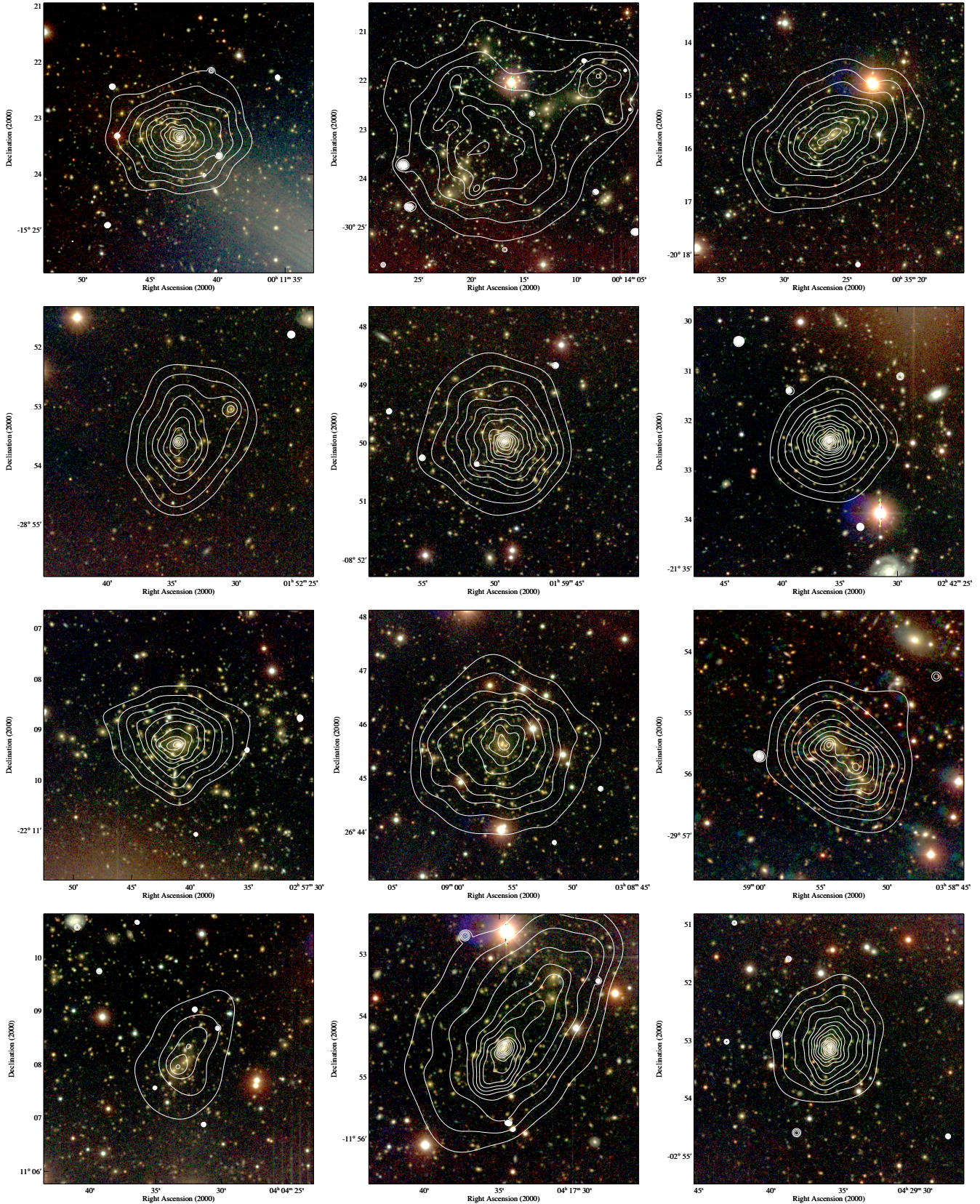


Figure 6. Contours of the X-ray surface brightness in the 0.5–7 keV band as observed with Chandra/ACIS-I overlaid on colour images obtained with the UH2.2m telescope (V,R,I; 12 min per filter). All images span 1.5 Mpc on the side at the cluster redshift. Contours are spaced logarithmically at the same levels for all images, except for MACSJ2140.2–2339 for which only ACIS-S data are available; we omit the lowest two contour levels to account for the higher background of the ACIS-S detector. The Chandra data were adaptively smoothed to 3σ significance using the ASMOOTH algorithm of Ebeling, White, and Rangarajan (2005). The final two panels (framed in black and spanning 4.5 arcmin on the side) show two of the three candidates revealed as point sources by Chandra and thence removed from the sample (for the third candidate listed in Table 1 and shown in Fig. 3 we do not have a UH2.2m colour image).

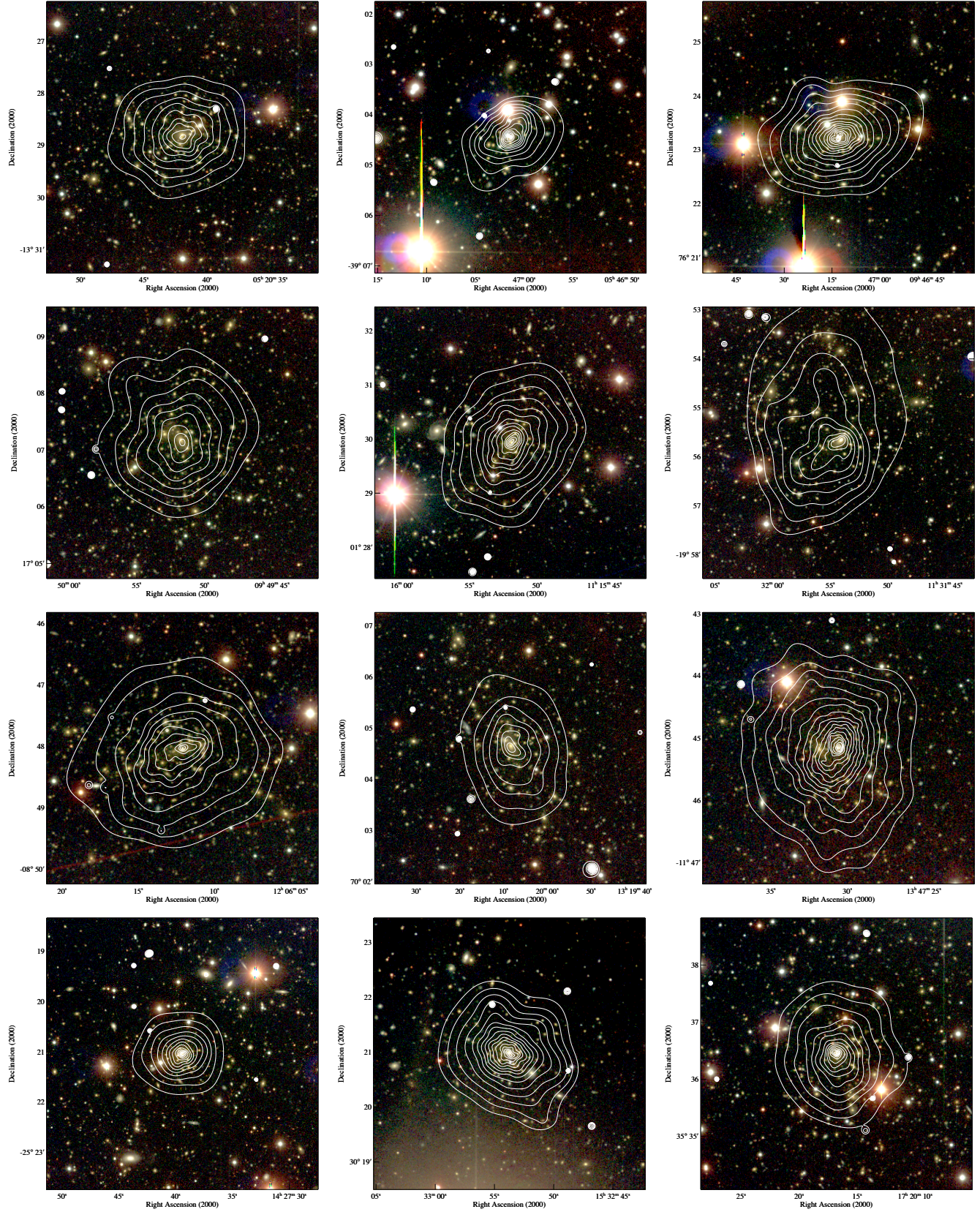


Figure 6 – *continued*

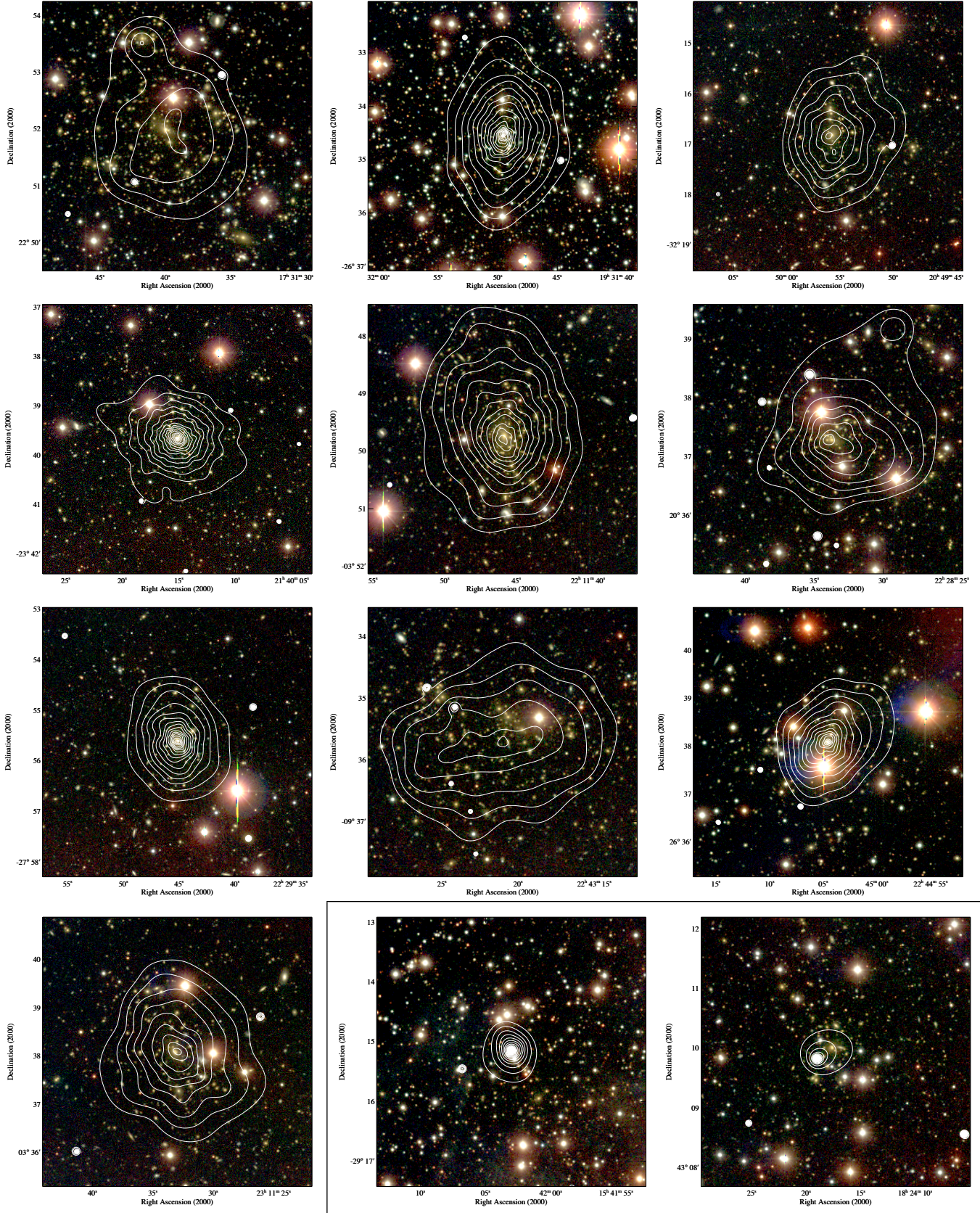


Figure 6 – continued

(Ebeling et al. 1998, 2000; Böhringer et al. 2004) and the complete set of the 12 most distant MACS clusters ($z > 0.5$) released earlier (Ebeling et al. 2007), the sample presented here allows cosmological and astrophysical studies of the properties and evolution of the most massive galaxy clusters over a contiguous redshift range from $z \sim 0$ to $z = 0.7$ (Allen et al. 2003, 2004, 2008; Ebeling et al. 2009; Mantz et al. 2008, 2010a,b, Rapetti et al. 2009). For convenience, we have supplied a tabulated version of the appropriate selection function.

ACKNOWLEDGMENTS

We thank many incarnations of the Chandra peer-review panel and of the University of Hawaii's telescope time allocation committee for their support, trust, and patience. HE gratefully acknowledges financial support from NASA LTSA grant NAG 5-8253 and SAO grants GO2-3168X, GO5-6133X, and GO0-11140X. ACE thanks the Royal Society for generous support during the identification phase of the MACS project. Parts of this work received support from the U.S. Department of Energy under contract number DE-AC02-76SF00515, as well as from SAO grants DD5-6031X, GO7-8125X and GO8-9118X. AM was supported by a Stanford Graduate Fellowship and an appointment to the NASA Postdoctoral Program, administered by Oak Ridge Associated Universities through a contract with NASA.

REFERENCES

- Allen S.W. et al. 1992, MNRAS, 259, 67
 Allen S.W., Schmidt R.W., Fabian A.C., Ebeling H. 2003, MNRAS, 342, 287
 Allen S.W., Schmidt R.W., Ebeling H., Fabian A.C., van Speybroeck L. 2004, MNRAS, 353, 457
 Allen S.W., Rapetti D.A., Schmidt R.W., Ebeling H., Morris R.G., Fabian A.C. 2008, MNRAS, 383, 879
 Atrio-Barandela F., Kashlinsky A., Kocevski D., Ebeling H. 2008, ApJ, 675, L57
 Böhringer H. et al. 2004, A&A, 425, 367
 Bonafede A. et al. A&A, 503, 707
 Bradač M., Allen S.W., Treu T., Ebeling H., Massey R., Morris R.G., von der Linden A., Applegate D. 2008, ApJ, 687, 959
 Burenin R.A., Vikhlinin A., Hornstrup A., Ebeling H., Quintana H., Mescheryakov A. 2007, ApJS, 172, 561
 Clowe D., Bradač M., Gonzalez A.H., Markevitch M., Randal S.W., Jones C., Zaritsky D. 2006, ApJ, 648, L109
 Crawford C.S., Edge A.C., Fabian A.C., Allen S.W., Böhringer H., Ebeling H., McMahon R.G., Voges W. 1995, MNRAS, 274, 75
 Crawford C.S., Allen S.W., Ebeling H., Edge A.C., Fabian A.C. 1999, MNRAS, 306, 857
 Cruddace R. et al. 2002, ApJS, 140, 239
 De Grandi S. et al. 1999, ApJ, 514, 148
 Ebeling H., Voges W., Böhringer H., Edge A.C., Huchra J.P., Briel U.G. 1996, MNRAS, 281, 799
 Ebeling H., Voges W., Böhringer H., Edge A.C., Huchra J.P., Briel U.G. 1997, ApJ, 479, L101
 Ebeling H., Edge A.C., Böhringer H., Allen S.W., Crawford C.S., Fabian A.C., Voges W., Huchra J.P. 1998, MNRAS, 301, 881
 Ebeling H., Edge A.C., Allen S.W., Crawford C.S., Fabian A.C., Huchra J.P. 2000, MNRAS, 318, 333
 Ebeling H., Edge A.C., Henry J.P. 2001, ApJ, 553, 668
 Ebeling H., Mullis C.R., Tully R.B. 2002, ApJ, 580, 774
 Ebeling H., Barrett E., Donovan D. 2004, ApJ, 609, L49
 Ebeling H., Barrett E., Donovan D., Ma C.-J., Edge A.C., van Speybroeck L. 2007, ApJ, 661, L33
 Ebeling H., Ma C.-J., Kneib J.-P., Jullo E., Courtney N.J.D., Barrett E., Edge A.C., Le Borgne J.-F. 2009, MNRAS, 395, 1213
 Edge A.C., Ebeling H., Bremer M., Röttgering H., van Haarlem M., Rengelink R., Courtney N. 2003, MNRAS, 339, 913
 Gioia I. & Luppino G.A. 1994, ApJS, 94, 583
 Hicks A.K. et al. 2008, ApJ, 680, 1022
 Horesh A., Maoz D., Ebeling H., Seidel G., Bartelmann M. 2009, MNRAS, submitted
 Horner D.J. et al. 2008, ApJS, 176, 376
 Hudson M.J. & Ebeling H. 1997, ApJ, 479, 621
 Kartaltepe J.S., Ebeling H., Ma C.-J., Donovan D. 2008, MNRAS, 389, 1240
 Kashlinsky A., Atrio-Barandela F., Kocevski D., Ebeling H. 2008, ApJ, 686, L49
 Kocevski D.D., Mullis C.R., Ebeling H. 2004, ApJ, 608, L49
 Kocevski D.D. & Ebeling H. 2006, ApJ, 368, 769
 Kocevski D.D., Ebeling H., Mullis C.R., Tully R.B. 2007, ApJ, 662, 224
 LaRoque S.J. et al. 2003, ApJ, 583, 559
 Ma C.-J., Ebeling H., Donovan D., Barrett E. 2008, ApJ, 684, 160
 Ma C.-J., Ebeling H., Barrett E. 2009, ApJ, 693, L56
 Mantz A., Allen S.W., Ebeling H., Rapetti D. 2008, MNRAS, 387, 1179
 Mantz A., Allen S.W., Rapetti D., Ebeling H. 2010a, MNRAS, submitted
 Mantz A., Allen S.W., Ebeling H., Rapetti D. 2010b, MNRAS, submitted
 Oke J.B., Postman M., Lubin L.M. 1998, AJ, 116, 549
 Perlmutter S. et al. 2002, ApJS, 140, 265
 Rapetti D., Allen S.W., Mantz A., Ebeling H. 2009, MNRAS, 400, 699
 Romer A.K. 1994, PhD thesis, University of Edinburgh
 Ruderman J.T. & Ebeling H. 2005, ApJ, 623, L81
 Schuecker P. et al. A&A, 368, 86
 Smail I. et al. 2007, ApJ, 654, L33
 Smith G.P., Kneib J.-P., Ebeling H., Czoske O., Smail I. 2001, ApJ, 552, 493
 Smith G.P., Kneib J.-P., Smail I., Mazzotta P., Ebeling H., Czoske O. 2005, MNRAS, 359, 417
 Smith G.P. et al. 2009, ApJL, in press
 Stanek R., Evrard A.E., Böhringer H., Schuecker P., Nord B. 2006, ApJ, 648, 956
 Stocke J.T., Morris S.L., Gioia I.M., Maccacaro T., Schild R., Wolter A., Fleming T., Henry J.P. 1991, ApJS, 76, 813
 Stott J.P., Smail I., Edge A.C., Ebeling H., Smith G.P., Kneib J.-P., Pimbblet K.A. 2007, ApJ, 661, 95
 Stott J.P., Edge A.C., Smith G.P., Swinbank A.M., Ebeling H. 2008, MNRAS, 384, 1502
 Trümper J. 1983, Adv. Space Res., 27, 1404
 van Haarlem M.P., Frenk C.S., White S.D.M. 1997, MNRAS, 287, 817
 van Weeren R.J. et al. 2009, A&A, 506, 1083
 Vikhlinin A. et al. 2009, ApJ, 692, 1033
 Voges W. et al. 1999, A&A, 349, 389
 Wright A., Ables J.G. & Allen D.A. 1983, MNRAS, 205, 793